J|A|C|S
ARTICLES

Published on Web 11/17/2008

Protein Side-Chain Dynamics As Observed by Solution- and Solid-State NMR Spectroscopy: A Similarity Revealed

Vipin Agarwal,[†] Yi Xue,[‡] Bernd Reif,*[,†] and Nikolai R. Skrynnikov*[,‡]

Forschungsinstitut für Molekulare Pharmakologie (FMP), Robert-Rössle-Str. 10, 13125 Berlin, Germany, and Department of Chemistry, Purdue University, 560 Oval Drive, West Lafayette, Indiana 47907-2084

Received June 12, 2008; E-mail: reif@fmp-berlin.de; nikolai@purdue.edu

Abstract: In this paper, we seek to compare the internal dynamics of a small globular protein, SH3 domain from α-spectrin, in solution and in a crystalline state. The comparison involves side-chain methyl ^{13}C R_1 relaxation rates that are highly sensitive to local dynamics in the vicinity of the methyl site. To conduct the relaxation measurements, protein samples have been prepared using specially labeled α-ketoisovalerate precursors, resulting in selective incorporation of the $^{1}H-^{13}C$ spin pair in one or both methyl groups of the valine and leucine side chains. The sparse labeling pattern in an otherwise deuterated sample makes it possible to record high-resolution ^{13}C, ^{1}H solid-state spectra using magic angle spinning experiment with a MAS frequency of 22 kHz. Furthermore, this labeling scheme avoids proton-driven $^{13}C-^{13}C$ spin-diffusion effects, thus allowing for accurate measurements of ^{13}C R_1 relaxation in the individual methyl groups. While the relaxation response from a polycrystalline sample is generally expected to be multiexponential, we demonstrate both theoretically and experimentally that in this particular case the relaxation profiles are, in excellent approximation, monoexponential. In fact, solid-state relaxation data can be interpreted in a model-free fashion, similar to solution data. Direct comparison between the experimentally measured solid and solution rates reveals a strong correlation, $r = 0.94$. Furthermore, when solution rates are corrected for the effect of the overall molecular tumbling (quantified on the basis of the solution ^{15}N relaxation data), the results are in one-to-one agreement with the solid-state rates. This finding indicates that methyl dynamics in the solution and solid samples are quantitatively similar. More broadly, it suggests that the entire dynamic network, including motions of side chains in the protein hydrophobic core and backbone motions, is similar. This result opens interesting possibilities for combined interpretation of solid- and solution-state relaxation data, potentially leading to a detailed characterization of internal protein dynamics on a wide range of time scales.

Introduction

X-ray crystallography has an outstanding record of solving protein structures. Importantly, crystallographic coordinates proved to be highly consistent with the structures solved by solution NMR. In fact, X-ray coordinates are generally favored as structural models for interpreting NMR data.[1,2] The realization that crystal structures provide valid models for proteins in the native solution-like environment effectively laid a foundation for modern structural biology.

Having made this observation about the structure, one can ask the same question about the dynamics: is there a substantial similarity between the internal protein motions that occur in the crystalline sample and the solution sample? The fact that the structures are similar augurs well for dynamics. There is also a large body of experimental evidence suggesting the presence of solution-like dynamics in protein crystals or, more generally, in hydrated solid samples. This includes the evidence of enzymatic catalysis[3] and ligand binding[4] in solids, crystallographic B-factors,[5] the occurrence of alternate conformations in crystallographic models,[6] as well as ample evidence from solid-state NMR line shape analyses and relaxation studies.[7,8] Solid-state NMR, in particular, can be employed in conjunction with solution NMR to test the similarity hypothesis. So far, however, few studies pursued a quantitative comparison.[9−12] With the advent of high-resolution triple-resonance MAS experiments,[13−15] a systematic quantitative comparison becomes feasible.[16−18]

[†] FMP.
[‡] Purdue University.

(1) Hu, J. S.; Bax, A. *J. Am. Chem. Soc.* **1997**, *119*, 6360–6368.
(2) Bax, A. *Protein Sci.* **2003**, *12*, 1–16.
(3) Careri, G.; Gratton, E.; Yang, P. H.; Rupley, J. A. *Nature* **1980**, *284*, 572–573.
(4) Chen, L. Y.; Rydel, T. J.; Gu, F.; Dunaway, C. M.; Pikul, S.; Dunham, K. M.; Barnett, B. L. *J. Mol. Biol.* **1999**, *293*, 545–557.
(5) Tilton, R. F.; Dewan, J. C.; Petsko, G. A. *Biochemistry* **1992**, *31*, 2469–2481.
(6) Svensson, L. A.; Sjölin, L.; Gilliland, G. L.; Finzel, B. C.; Wlodawer, A. *Proteins: Struct., Funct., Bioinf.* **1986**, *1*, 370–375.
(7) Torchia, D. A. *Annu. Rev. Biophys. Bioeng.* **1984**, *13*, 125–144.
(8) McDermott, A. E. *Curr. Opin. Struct. Biol.* **2004**, *14*, 554–561.
(9) Cole, H. B. R.; Torchia, D. A. *Chem. Phys.* **1991**, *158*, 271–281.
(10) Tamura, A.; Matsushita, M.; Naito, A.; Kojima, S.; Miura, K. I.; Akasaka, K. *Protein Sci.* **1996**, *5*, 127–139.
(11) Mack, J. W.; Usha, M. G.; Long, J.; Griffin, R. G.; Wittebort, R. J. *Biopolymers* **2000**, *53*, 9–18.
(12) Rozovsky, S.; McDermott, A. E. *J. Mol. Biol.* **2001**, *310*, 259–270.

In this study, we focus on the motion of side chains in a hydrophobic core of a globular protein. We contend that the dynamic behavior of the hydrophobic core in a well-hydrated crystalline sample strongly resembles the one that is observed in solution. To test this hypothesis, which is dubbed the "similarity hypothesis", is the main objective of our work.

In assessing the similarity hypothesis for the protein hydrophobic core, one should bear in mind two important considerations. (*i*) The core is ensconced in a well-structured backbone scaffold. This scaffold, which defines the structural "frame" for the motion of the hydrophobic side chains, does not change upon the transition from solution to crystal. (*ii*) The dynamics of the protein are dictated by solvation water.[19] Water unlocks the electrostatic contacts on the protein surface and recruits polar groups into a highly dynamic network.[20,21] The resulting mobility is transmitted then to the protein backbone and further on to the hydrophobic core. From the perspective of this study, it is important that a large reservoir of solvation water is retained upon protein crystallization.

Obviously, one factor can potentially undermine the similarity hypothesis—crystal contacts. Upon crystallization, the solvent-accessible surface of the protein is typically reduced by 25%[22] (in the case of the protein investigated in this study, the SH3 domain from chicken α-spectrin, the solvent-accessible area is reduced by 30%[23]). Below we offer some tentative arguments suggesting that crystal contacts have only a limited effect on the dynamics of the hydrophobic core.

It has been established using a variety of methods (including NMR line shape analyses, relaxation studies, and hydrogen exchange measurements) that the onset of native dynamics in globular proteins occurs already at a very modest level of hydration.[20,24,25] Further hydration, up to a saturation point, causes little change in the dynamic behavior. From this perspective, the crystalline environment, which ensures ca. 70% solvation of the protein surface, appears to be conducive to native-like internal motions. Note also that the crystal contacts are formed largely by hydrophilic side chains that retain substantial flexibility at the contact interface.[26] Furthermore, the perturbations induced by the crystal contacts seem to be limited to the surface layer and do not propagate into the hydrophobic core.[27] Finally, it is worth pointing out that the problem of protein−matrix interaction is not limited to dynamics studies by solid-state NMR. This problem is also present in the studies of protein dynamics using residual dipolar couplings.[28] Indeed, residual dipolar couplings arise from molecular configurations where protein is directly interacting with bicelle, phage, etc. These interactions are specific with respect to protein topology and/or charge distribution, just like crystal contacts. Ignoring these interactions, as is customary in the RDC-based dynamics studies, apparently has little or no adverse effect on the analyses. All these arguments, however, are of tentative nature. Ultimately, it is the experimental results (such as described below) that shed light on this problem.

To test the similarity hypothesis, we chose to compare the relaxation behavior of side-chain methyl groups. The favorable spectroscopic properties of methyls are well-documented.[29] For the solid-state studies, it is particularly important that methyl sites can be selectively labeled with relative ease.[30−33] The presence of the efficient relaxation mechanism associated with the rotation of the methyl group makes the interpretation of the solid-state data more straightforward than for other protein sites (it also helps that methyl protons do not exchange with the solvent).[34] Since methyl spins relax much faster than most other spins in solids, shorter recycling delays can be employed in the pulse sequences.

Our first attempt to compare methyl dynamics using ^{2}H relaxation rates was only partially successful.[17] As it turned out, even at high MAS speed, ^{2}H spins are susceptible to spin-diffusion effects.[35] This leads to partial mixing of the relaxation responses from ^{2}H spins in different methyl and non-methyl positions.[17] In the current study, we opted for ^{13}C measurements.[36−38] Using the labeling protocol developed in the Kay laboratory,[30] ^{13}C spins are incorporated in a highly selective fashion in the ^{2}H,^{12}C-labeled sample. As confirmed both experimentally and by simulations, this labeling scheme avoids the troublesome spin-diffusion effects.

To draw a comparison between solution and solids, we focus on the ^{13}C spin−lattice relaxation rates. It is easy to demonstrate that, both in solution and in solids, methyl ^{13}C R_1 rates are dominated by the fast methyl rotation. Thus, a direct comparison is possible between the two respective data sets. The high degree of correlation found in our analysis, $r = 0.94-0.95$, offers strong evidence in favor of the similarity hypothesis.

(13) Pauli, J.; van Rossum, B.; Förster, H.; de Groot, H. J. M.; Oschkinat, H. *J. Magn. Reson.* **2000**, *143*, 411–416.
(14) McDermott, A.; Polenova, T.; Böckmann, A.; Zilm, K. W.; Paulsen, E. K.; Martin, R. W.; Montelione, G. T. *J. Biomol. NMR* **2000**, *16*, 209–219.
(15) Chevelkov, V.; Rehbein, K.; Diehl, A.; Reif, B. *Angew. Chem., Int. Ed.* **2006**, *45*, 3878–3881.
(16) Lorieau, J. L.; McDermott, A. E. *J. Am. Chem. Soc.* **2006**, *128*, 11505–11512.
(17) Reif, B.; Xue, Y.; Agarwal, V.; Pavlova, M. S.; Hologne, M.; Diehl, A.; Ryabov, Y. E.; Skrynnikov, N. R. *J. Am. Chem. Soc.* **2006**, *128*, 12354–12355.
(18) Chevelkov, V.; Zhuravleva, A. V.; Xue, Y.; Reif, B.; Skrynnikov, N. R. *J. Am. Chem. Soc.* **2007**, *129*, 12594–12595.
(19) Frauenfelder, H.; Gratton, E. *Methods Enzymol.* **1986**, *127*, 207–216.
(20) Gregory, R. B.; Gangoda, M.; Gilpin, R. K.; Su, W. *Biopolymers* **1993**, *33*, 513–519.
(21) Zanotti, J. M.; Bellissent-Funel, M. C.; Parello, J. *Biophys. J.* **1999**, *76*, 2390–2411.
(22) Islam, S. A.; Weaver, D. L. *Proteins: Struct., Funct., Bioinf.* **1990**, *8*, 1–5.
(23) Chevelkov, V.; Faelber, K.; Diehl, A.; Heinemann, U.; Oschkinat, H.; Reif, B. *J. Biomol. NMR* **2005**, *31*, 295–310.
(24) Andrew, E. R. *Polymer* **1985**, *26*, 190–192.
(25) Rupley, J. A.; Careri, G. *Adv. Protein Chem.* **1991**, *41*, 37–172.
(26) Kossiakoff, A. A.; Randal, M.; Guenot, J.; Eigenbrot, C. *Proteins: Struct., Funct., Bioinf.* **1992**, *14*, 65–74.
(27) Jacobson, M. P.; Friesner, R. A.; Xiang, Z. X.; Honig, B. *J. Mol. Biol.* **2002**, *320*, 597–608.
(28) Louhivuori, M.; Otten, R.; Lindorff-Larsen, K.; Annila, A. *J. Am. Chem. Soc.* **2006**, *128*, 4371–4376.
(29) Ollerenshaw, J. E.; Tugarinov, V.; Skrynnikov, N. R.; Kay, L. E. *J. Biomol. NMR* **2005**, *33*, 25–41.
(30) Goto, N. K.; Gardner, K. H.; Mueller, G. A.; Willis, R. C.; Kay, L. E. *J. Biomol. NMR* **1999**, *13*, 369–374.
(31) Morcombe, C. R.; Gaponenko, V.; Byrd, R. A.; Zilm, K. W. *J. Am. Chem. Soc.* **2005**, *127*, 397–404.
(32) Tugarinov, V.; Kanelis, V.; Kay, L. E. *Nat. Protoc.* **2006**, *1*, 749–754.
(33) Schubert, M.; Manolikas, T.; Rogowski, M.; Meier, B. H. *J. Biomol. NMR* **2006**, *35*, 167–173.
(34) Giraud, N.; Sein, J.; Pintacuda, G.; Böckmann, A.; Lesage, A.; Blackledge, M.; Emsley, L. *J. Am. Chem. Soc.* **2006**, *128*, 12398–12399.
(35) Alla, M.; Eckman, R.; Pines, A. *Chem. Phys. Lett.* **1980**, *71*, 148–151.
(36) Wittebort, R. J.; Rothgeb, T. M.; Szabo, A.; Gurd, F. R. N. *Proc. Natl. Acad. Sci. U.S.A.* **1979**, *76*, 1059–1063.
(37) Richarz, R.; Nagayama, K.; Wuthrich, K. *Biochemistry* **1980**, *19*, 5189–5196.
(38) Straus, S. K.; Bremi, T.; Ernst, R. R. *J. Biomol. NMR* **1997**, *10*, 119–128.

While methyl rotation *per se* may be of limited interest, the rate of rotation is highly sensitive to the dynamics around the methyl site.[39,40] Thus, we view this result as an indication of a general similarity between the internal dynamics in the two samples. As discussed in the concluding section, the similarity hypothesis provides a justification for combined interpretation of the solid- and solution-state data.[18] This new approach is expected to be useful for characterizing various forms of motion, including the elusive nanosecond time-scale dynamics.

Materials and Methods

Samples. The study was conducted on a small globular protein, chicken α-spectrin SH3 domain (α-spc SH3), which has been well-characterized by both solution- and solid-state NMR.[41−43] Selective labeling of Leu and Val methyl groups was achieved by adding an α-ketoisovalerate to the expression media[30] (α-ketobutyrate[44] was not used since there is only one Ile residue in α-spc SH3). For solution measurements, the sample was prepared using α-ketoisovalerate with the labeling scheme $^{13}CHD_2$-CH($^{13}CHD_2$)-CO-COO$^-$. The compound was purchased from Isotec (cat. no. 634379) and deuterated at the 3 position as described previously.[30] For solid experiments, the $^{13}CHD_2$-CD(CD_3)-CO-COO$^-$ variant[45] was used (Cambridge Isotope Laboratories, cat. no. 7354). Using this precursor, each Val and Leu side chain is expressed with one labeled and one unlabeled methyl group, thus reducing the probability of (proton-driven) $^{13}C-^{13}C$ spin diffusion. The protein was expressed in D_2O-based media containing 100 mg/L of labeled α-ketoisovalerate and 2 g/L deuterated D-glucose, thus ensuring [U-^{2}H,^{12}C] background. One gram/liter $^{15}NH_4Cl$ was added to the media to label the amide sites. In our hands, the yields were in the range of 10−20 mg/L.

The solution sample was dissolved in 90% H_2O−10% D_2O, unbuffered, pH 3.5, to the concentration of 2.4 mM. Solid-state samples were crystallized from 10% H_2O−90% D_2O by raising the pH to 7.5, as described previously.[13] Two samples were used in the solid-state measurements. The pilot sample contained ca. 1 mg of the protein material packed in a 3.2 mm rotor. The subsequently produced main sample contained ca. 8.5 mg of the protein. The residual content of the (backbone and side-chain) amine protons in the two samples was at the level of ca. 10 and 15%, respectively (in the latter case, the labile protons were not fully exchanged). Note that complete deuteration of exchangeable sites would be beneficial for the solid-state measurements aimed at methyl groups (see below). Although the pilot sample is in certain ways preferable (lower proton density, better sample homogeneity), the main sample offers substantially better sensitivity. In what follows, the discussion is limited to the data from the main sample since they are significantly more precise. Additional information on the pilot sample can be found in the Supporting Information.

NMR Experiments. Both solution- and solid-state measurements were conducted at 20 °C; in the latter case, the temperature was carefully calibrated using methanol chemical shifts,[46] and the uncertainty was estimated to be ±2 °C. All solid and solution data were collected at the static magnetic field 14.1 T (600 MHz).

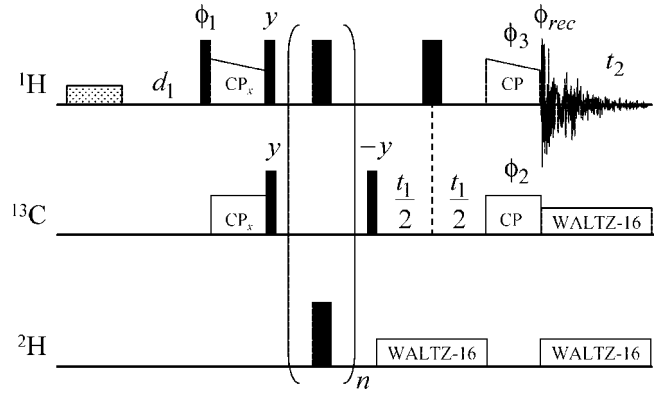

Figure 1. Solid-state NMR experiment for measuring carbon R_1 relaxation rates in side-chain methyl $^{13}CHD_2$ groups. The rf carrier on the ^{1}H channel was set to 4.8 ppm except for the duration of the first pulse (shaded outline) where the carrier was transferred to 1.8 ppm. The rf carriers on the ^{13}C and ^{2}H channels were positioned at 24 and 3 ppm, respectively. Narrow (wide) pulses were applied with a flip angle of 90° (180°) and the field strengths of 49, 38, and 64 kHz for the ^{1}H, ^{13}C, and ^{2}H channels, respectively. During the first CP element (duration 2 ms), a constant rf field of 34 kHz was applied on the ^{13}C channel, while the rf field on the proton channel was swept from 60 to 45 kHz, achieving a frequency match at (−1) spinning sideband.[51,52] The second CP element was made shorter, 1 ms, to avoid a possibility of long-range magnetization transfer, with slightly higher rf field amplitudes. WALTZ-16 decoupling[53] on the ^{13}C and ^{2}H channels was applied with the field strengths of 2.7 and 2.0 kHz, respectively. The decay curves were sampled at the time intervals $T_{rel} = n \times 40$ ms, with ^{1}H and ^{2}H 180° pulses applied every 40 ms in order to suppress cross-correlations[54,55] (note that for rapidly relaxing ^{2}H spin cross-correlations are expected to be largely self-decoupled). Frequent application of the ^{1}H 180° pulses leads to efficient suppression of the residual water signal. Furthermore, it achieves the constant degree of saturation for methyl ^{1}H magnetization, which in turn ensures that the ^{13}C magnetization relaxes toward an invariant "steady state". The recycling delay d_1 between the two consecutive scans was 2.5 s. The pulse applied prior to d_1 (shaded outline, duration 2 ms, field strength 3.2 kHz) was intended to further saturate methyl ^{1}H magnetization and thus ensure identical starting conditions for spectra recorded with different durations of T_{rel}. The spectra were acquired as 4096 × 192 complex matrices with spectral widths of 60 060 and 3125 Hz in the ^{1}H and ^{13}C dimensions, respectively. The rf pulses have been applied with the phase x, unless indicated otherwise. The phase cycle was $\phi 1 = (y, -y)$, $\phi 2 = 2(x)2(-x)$, $\phi 3 = 4(x)4(-x)$, $\phi_{rec} = (x, -x, -x, x, -x, x, x, -x)$. Phase-sensitive detection in t_1 was achieved by means of TPPI.[56] The experimental time per T_{rel} point was from 4.5 to 8 h, depending on the duration of T_{rel}. The measurements were conducted using a 3.2 mm rotor at the spinning frequency of 22 kHz.

Solid-state methyl ^{13}C R_1 rates were measured using the sequence shown in Figure 1. In addition, the absence of $^{13}C-^{13}C$ spin-diffusion effects was confirmed by recording a 2D exchange spectrum. This latter control experiment made use of the pulse sequence which was similar to the one shown in Figure 1, with the following exceptions: (*i*) the evolution period t_1 and the relaxation (mixing) period T_{rel} were interchanged, and (*ii*) each of the two cross-polarization elements was replaced with the refocused INEPT. All experimental settings, such as the MAS frequency, rf power, etc., were the same as described in the caption of Figure 1.

Solution ^{13}C R_1 and $R_{1\rho}$ data were recorded using the pulse sequences fashioned from the standard ^{15}N experiments, as ap-

(39) Chatfield, D. C.; Augsten, A.; D'Cunha, C. *J. Biomol. NMR* **2004**, *29*, 377–385.
(40) Xue, Y.; Pavlova, M. S.; Ryabov, Y. E.; Reif, B.; Skrynnikov, N. R. *J. Am. Chem. Soc.* **2007**, *129*, 6827–6838.
(41) Blanco, F. J.; Ortiz, A. R.; Serrano, L. *J. Biomol. NMR* **1997**, *9*, 347–357.
(42) Pauli, J.; Baldus, M.; van Rossum, B.; de Groot, H.; Oschkinat, H. *ChemBioChem* **2001**, *2*, 272–281.
(43) Castellani, F.; van Rossum, B.; Diehl, A.; Schubert, M.; Rehbein, K.; Oschkinat, H. *Nature* **2002**, *420*, 98–102.
(44) Gardner, K. H.; Kay, L. E. *J. Am. Chem. Soc.* **1997**, *119*, 7599–7600.
(45) Lichtenecker, R.; Ludwiczek, M. L.; Schmid, W.; Konrat, R. *J. Am. Chem. Soc.* **2004**, *126*, 5348–5349.
(46) Aliev, A. E.; Harris, K. D. M. *Magn. Reson. Chem.* **1994**, *32*, 366–369.
(47) Farrow, N. A.; Muhandiram, R.; Singer, A. U.; Pascal, S. M.; Kay, C. M.; Gish, G.; Shoelson, S. E.; Pawson, T.; Forman-Kay, J. D.; Kay, L. E. *Biochemistry* **1994**, *33*, 5984–6003.
(48) Korzhnev, D. M.; Skrynnikov, N. R.; Millet, O.; Torchia, D. A.; Kay, L. E. *J. Am. Chem. Soc.* **2002**, *124*, 10743–10753.
(49) Hansen, D. F.; Kay, L. E. *J. Biomol. NMR* **2007**, *37*, 245–255.
(50) Tollinger, M.; Skrynnikov, N. R.; Mulder, F. A. A.; Forman-Kay, J. D.; Kay, L. E. *J. Am. Chem. Soc.* **2001**, *123*, 11341–11352.
(51) Metz, G.; Wu, X. L.; Smith, S. O. *J. Magn. Reson. Ser. A* **1994**, *110*, 219–227.
(52) Baldus, M.; Geurts, D. G.; Hediger, S.; Meier, B. H. *J. Magn. Reson. Ser. A* **1996**, *118*, 140–144.

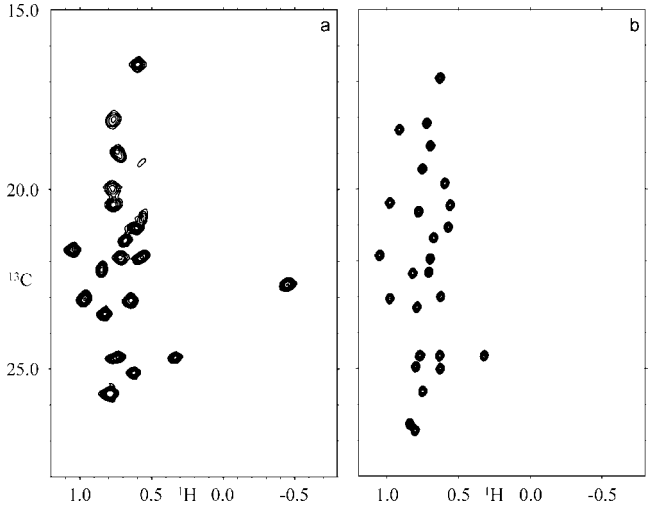

Figure 2. Spectra of α-spc SH3 from methyl ^{13}C R_1 relaxation measurements: (a) solid-state experiment, pulse sequence Figure 1, and (b) solution-state experiment, pulse sequence Figure S1a in the Supporting Information. The resonance assignments are shown in Figure S2 in the Supporting Information.

propriate for the two-spin $^{13}CHD_2$ system (see Figure S1 in the Supporting Information). In addition to ^{13}C measurements, ^{15}N relaxation data were collected in solution using the standard suite of experiments.[47−49] The absence of the R_{ex} contribution into transverse relaxation in all residues except Asp48 was confirmed by ^{15}N relaxation dispersion measurement.[50]

NMR Spectra. The solid-state spectrum recorded by means of the pulse sequence Figure 1 at a MAS frequency of 22 kHz is shown in Figure 2a. Shown alongside is the spectrum from the solution study (Figure 2b). As demonstrated previously, the use of the samples where ^{13}C,^{1}H-labeled methyl groups are incorporated in the otherwise ^{12}C,^{2}H-labeled proteins allows for recording of the MAS spectra with unusually high resolution, comparable to that of solution spectra.[31,57] The samples used in this study are particularly attractive because all labeled methyls are of $^{13}CHD_2$ variety. The labeling scheme involving a single isotopomer, as opposed to a mixture, allows for all proton magnetization to be fully utilized by the pulse sequence. Furthermore, $^{13}CHD_2$ is preferable to other isotopomers as it offers better spectroscopic properties.[57] The result is the solid-state spectrum that combines high resolution with high sensitivity.

The quantitative similarity between the solid- and solution-state chemical shifts in small globular proteins has been well-documented.[9,14,58−62] A good agreement is also observed here for stereospecifically assigned methyls (see Figure S3 in the Supporting Information). The rmsd between the solid and solution shifts amounts to 0.28 and 0.5 ppm for proton and carbon, respectively. This is in line with what has been previously reported for backbone $^{1}H^{\alpha}$ and $^{13}C^{\alpha}$ spins. One distinct outlier is the resonance from Leu8 $\delta 2$, which appears at (0.77, 24.6) ppm in solution spectrum versus (−0.50, 22.6 ppm) in the solid spectrum. This methyl forms a close crystal contact: according to the crystallographic coordinates 1U06,[23] the distance between Leu8 $C^{\delta 2}$ and the nearest heavy atom from another protein molecule is 3.9 Å. If this outlier is excluded, the agreement between the solid- and solution-state shifts improves to 0.07, 0.3 ppm. Considering the sensitivity of chemical shifts to subtle structural changes, this result nicely confirms the invariance of the protein structure.

Inspection of the solid-state spectrum (Figure 2a) reveals a large disparity between the intensities of individual peaks. There is an order-of-magnitude difference between the weakest and the strongest peaks. Moreover, two peaks are barely identifiable, and resonances from two methyls cannot be found at all in the spectrum. This situation persists in the spectra recorded by means of HSQC- and HMQC-style solid-state sequences where the magnetization transfer is effected by scalar, rather than dipolar, interaction (results not shown). On the contrary, peak intensities in solution are essentially uniform and all resonances are at hand (Figure 2b).

What are the reasons for this disparity?

First, it appears that certain peaks in the solid-state spectra are attenuated due to side-chain χ_1, χ_2 rotameric jumps occurring on a nanosecond−microsecond time scale. The high-resolution crystallographic structure 1U06 (resolution 1.49 Å)[23] contains three LV side chains that adopt alternate conformations: Val23, Leu31, and Val46. In the case of Val23, the time scale of the rotameric jumps is known to be in the range of 2−4 ns.[17] This process is sufficiently fast and, therefore, causes only a limited amount of relaxation broadening. In the case of Leu31 and Val46, the situation is less clear. Solution-state measurements fail to detect nanosecond time-scale motions in these side chains, which may indicate that the jumps occur on the time scale substantially longer than molecular tumbling, $\gg$5 ns.[17] Assuming for a moment that these two side chains indeed experience rotameric jumps on high nanosecond to low microsecond time scale, what would be the consequences of such dynamic process? From the perspective of solution spectroscopy, this process is "silent": the motion is much slower than molecular tumbling and, therefore, has no effect on dipolar or CSA relaxation, yet it is too fast to generate any appreciable exchange broadening R_{ex}. In solids, however, the tumbling is absent—as a result, slow rotameric jumps can efficiently modulate dipolar and CSA interactions, causing severe line broadening. This type of behavior can be readily reproduced by simulating MAS spectra of a two-spin system undergoing two-site exchange.[63] The described scenario is fully consistent with the experimental evidence. In the solution spectra, all methyl resonances from Leu31 and Val46 are accounted for and have the appearance of sharp, intense peaks. At the same time, in the solid spectra, two Leu31 peaks are barely detectable, whereas two Val46 resonances cannot be found at all. We believe that slow rotameric jumps are likely responsible for this situation.[61]

Second, the intensity of each individual peak in the solid-state spectrum appears to be inversely proportional to the local proton density around the corresponding methyl group. To demonstrate this trend, we calculated the effective distance between the protons from the given methyl group and the surrounding protons, $r_{HH'}^{eff} = (\Sigma_i 1/r_{HH'_i}^3)^{-1/3}$. The calculation was conducted using the coordinates 1U06; the explicit crystal lattice environment was constructed and added to the structure using the program WHAT IF.[64] The proton incorporation pattern was chosen to mimic the experimental conditions: one methyl proton per Val/Leu side chain, plus 10−15%

(53) Shaka, A. J.; Keeler, J.; Frenkiel, T.; Freeman, R. *J. Magn. Reson.* **1983**, *52*, 335–338.
(54) Palmer, A. G.; Skelton, N. J.; Chazin, W. J.; Wright, P. E.; Rance, M. *Mol. Phys.* **1992**, *75*, 699–711.
(55) Kay, L. E.; Nicholson, L. K.; Delaglio, F.; Bax, A.; Torchia, D. A. *J. Magn. Reson.* **1992**, *97*, 359–375.
(56) Marion, D.; Wüthrich, K. *Biochem. Biophys. Res. Commun.* **1983**, *113*, 967–974.
(57) Agarwal, V.; Diehl, A.; Skrynnikov, N.; Reif, B. *J. Am. Chem. Soc.* **2006**, *128*, 12620–12621.
(58) van Rossum, B. J.; Castellani, F.; Rehbein, K.; Pauli, J.; Oschkinat, H. *ChemBioChem* **2001**, *2*, 906–914.
(59) Bockmann, A.; Lange, A.; Galinier, A.; Luca, S.; Giraud, N.; Juy, M.; Heise, H.; Montserret, R.; Penin, F.; Baldus, M. *J. Biomol. NMR* **2003**, *27*, 323–339.
(60) Igumenova, T. I.; Wand, A. J.; McDermott, A. E. *J. Am. Chem. Soc.* **2004**, *126*, 5323–5331.
(61) Franks, W. T.; Zhou, D. H.; Wylie, B. J.; Money, B. G.; Graesser, D. T.; Frericks, H. L.; Sahota, G.; Rienstra, C. M. *J. Am. Chem. Soc.* **2005**, *127*, 12291–12305.
(62) Marulanda, D.; Tasayco, M. L.; Cataldi, M.; Arriaran, V.; Polenova, T. *J. Phys. Chem. B* **2005**, *109*, 18135–18145.
(63) Skrynnikov, N. R. *Magn. Reson. Chem.* **2007**, *45*, S161–S173.
(64) Vriend, G. *J. Mol. Graphics* **1990**, *8*, 52–56.

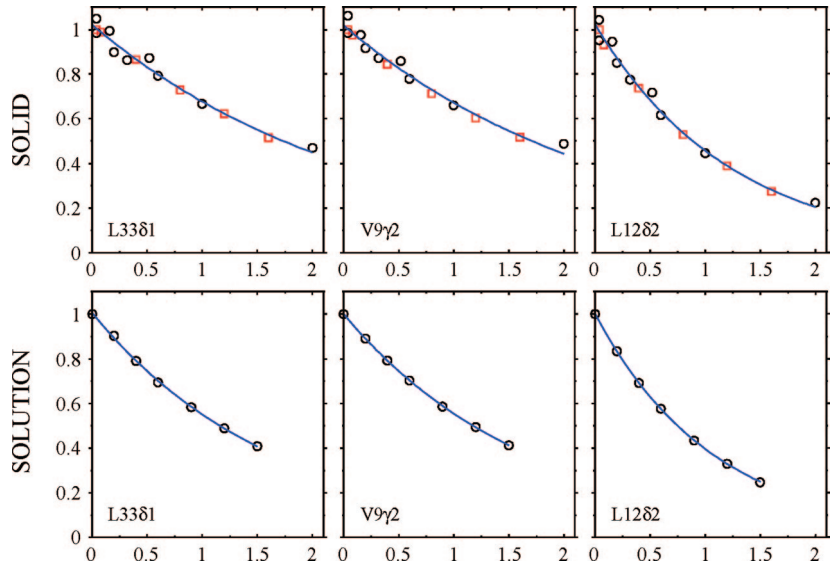

Figure 3. Representative methyl ^{13}C R_1 relaxation curves from solid- and solution-state measurements on α-spc SH3 (y axis: normalized peak volume; x axis: time T_{rel} in the units of seconds). In plotting the solid-state data, we distinguish six points sampled in the beginning of the experimental run (red squares) and nine points sampled toward the end of the experimental run (black circles). The observed pattern suggests that, with some improvement in hardware stability, it should be possible to record the relaxation profiles of excellent quality, comparable to that in solution. The uncertainties in the decay rates are estimated as a part of the single-exponential fitting routine.[47]

proton content at the exchangeable sites. As it turns out, the calculated $r_{HH'}^{eff}$ values show a significant correlation with the experimental peak intensities; the obtained correlation coefficients are 0.67 and 0.78 for the spectra shown in Figure 2a and Figure S2a in the Supporting Information, respectively. Thus, methyls with significant exposure to external protons give rise to weak, broadened peaks and vice versa.

Third, it appears that the spectrum Figure 2a suffers from a certain amount of inhomogeneous broadening. In fact, some of the mis-shapen peaks in this spectrum consist of two poorly resolved components. This behavior can be attributed to the sample inhomogeneity and the resulting variation in chemical shift. As might be expected, the bigger of the two solid samples is the one that is more affected (cf. Figure 2a and Figure S2a in the Supporting Information).

Clearly, there is a number of ways to improve the quality of the solid-state spectra. A significant improvement can be obtained by complete elimination of the exchangeable protons. The methyl proton pool, already dilute, can be further diluted by using a mixture of selectively protonated and perdeuterated precursors. Furthermore, sample homogeneity can be improved through a number of methods.[65] It is instructive to consider the results from a uniformly deuterated sample of α-spc SH3 with low-level proton background (ca. 8%).[66] Using this sample, we were able to achieve nearly uniform excitation of methyl resonances (apart from Leu31 and Val46 correlations that remained weak or undetectable). Raising the temperature from 20 to 33 °C led to significant deterioration in the overall signal-to-noise ratio of the spectrum. At the same time, the signals from Val46 became observable and the signals from Leu31 showed dramatic gains in intensity (consistent with the interpretation proposed above). This illustrates one of the possible approaches that can be taken to improve the conditions for observation of methyls. While there is room for improvement, the existing solid samples produced high-quality spectra that proved to be fully suitable for the purpose of relaxation measurements. The results of these measurements are discussed below.

Results and Interpretation

Comparing Solid- and Solution-State Relaxation. The typical methyl ^{13}C R_1 relaxation curves are shown in Figure 3. To select the representative data, all solid-state relaxation profiles were sorted according to the quality of the (single-exponential) fitting, and three entries, Leu33 $\delta1$, Val9 $\gamma2$, and Leu12 $\delta2$, were picked exactly from the middle of the sorted list. As a point of comparison, the solution relaxation curves for the same sites are shown alongside (Figure 3).

The results shown in Figure 3 raise some important questions. First, it is not *a priori* clear whether the results of the solid-state relaxation experiment are affected by the proton-driven $^{13}C-^{13}C$ spin diffusion.[67,68] Second, the relaxation profiles acquired from a polycrystalline sample are generally expected to be multiexponential.[69,70] We defer the discussion of these questions until the next section. At this point, we satisfy ourselves with a general observation that the R_1 relaxation of methyl spins is dominated by methyl group rotation both in solids *and* in liquids (in the case of liquids, this is particularly true of macromolecules).[71−74] Thus, if the similarity hypothesis

(65) Jakeman, D. L.; Mitchell, D. J.; Shuttleworth, W. A.; Evans, J. N. S. *J. Biomol. NMR* **1998**, *12*, 417–421.
(66) Agarwal, V.; Reif, B. *J. Magn. Reson.* **2008**, *194*, 16–24.
(67) Meier, B. H. Polarization transfer and spin diffusion. In *Advances in Magnetic and Optical Resonance*; Warren, W. S., Ed.; Academic Press: San Diego, CA, 1994; Vol. 18, pp 1−116.
(68) Grommek, A.; Meier, B. H.; Ernst, M. *Chem. Phys. Lett.* **2006**, *427*, 404–409.
(69) Torchia, D. A.; Szabo, A. *J. Magn. Reson.* **1982**, *49*, 107–121.
(70) Giraud, N.; Blackledge, M.; Goldman, M.; Böckmann, A.; Lesage, A.; Penin, F.; Emsley, L. *J. Am. Chem. Soc.* **2005**, *127*, 18190–18210.
(71) Akasaka, K.; Ganapathy, S.; McDowell, C. A.; Naito, A. *J. Chem. Phys.* **1983**, *78*, 3567–3572.
(72) Batchelder, L. S.; Niu, C. H.; Torchia, D. A. *J. Am. Chem. Soc.* **1983**, *105*, 2228–2231.
(73) Ishima, R.; Petkova, A. P.; Louis, J. M.; Torchia, D. A. *J. Am. Chem. Soc.* **2001**, *123*, 6164–6171.
(74) Muhandiram, D. R.; Yamazaki, T.; Sykes, B. D.; Kay, L. E. *J. Am. Chem. Soc.* **1995**, *117*, 11536–11544.

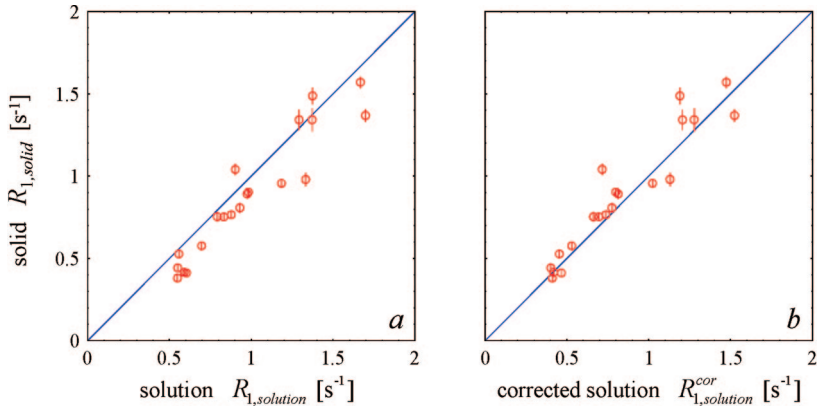

Figure 4. Correlations between the methyl ^{13}C R_1 relaxation rates determined from solid- and solution-state studies of α-spc SH3. (a) $R_{1,solid}$ and $R_{1,solution}$ directly as measured experimentally; (b) $R_{1,solid}$ directly as measured experimentally, $R^{cor}_{1,solution}$ corrected to remove the contribution from the overall protein tumbling. The correction has been calculated using the additional solution-state data: methyl ^{13}C $R_{2,solution}$ and the standard set of backbone ^{15}N relaxation data.

is upheld, then one expects to find a strong correlation between the solid- and solution-state methyl ^{13}C R_1 rates.

The correlation plot for the R_1 rates is shown in Figure 4a. Note that the experimentally measured rates are used as is, without any kind of alterations. The correlation coefficient obtained in this graph, $r = 0.94$, provides an instant validation for the similarity hypothesis. As one may expect, the points in Figure 4a fall mainly below the diagonal. The reason for this is that the $R_{1,solution}$ rates contain an additional (modest) contribution from the protein overall tumbling, which is absent from the solid rates. In the following sections, we turn to a quantitative interpretation of the results and, in particular, subtract out the tumbling contribution.

Potential Complications: Proton-Driven ^{13}C−^{13}C Spin Diffusion. Both in solids and in solution, the relaxation measurements can be compromised by spin-diffusion effects. In solutions, it is only ^{1}H relaxation that is adversely affected.[75,76] In solids, low-γ nuclei such as ^{2}H and ^{15}N can be impacted as well.[17,77,78] In essence, during the time T_{rel}, the magnetization is exchanged between multiple spins so that the measured decay profiles are no longer representative of the specific spin sites, but rather involve responses from multiple sites. Because of the size of the spin network involved, it is difficult to analyze this effect; as a result, the quantitative character of the study is lost.

To clarify the role of proton-driven ^{13}C−^{13}C spin diffusion (PDSD) in the context of our solid-state measurements, we first turned to the experimental evidence. The PDSD transfer can be readily detected via a simple 2D exchange experiment.[67,79] While these experiments typically utilize heteronuclear detection,[78,80] it is also possible to implement a version with proton detection (this requires a sample with high degree of deuteration, such as used in our study). The details of the pulse sequence are described in Materials and Methods. The spectrum recorded in 14 h using the mixing time of 1.2 s produced no evidence of PDSD cross-peaks. We conclude that no appreciable PDSD transfer takes place on the time scale of the methyl ^{13}C spin−lattice relaxation (cf. Figure 3).

To identify the main factors that govern PDSD transfer in the context of our solid-state experiments, we undertook a series of numeric simulations. Specifically, we focused on the methyl pairs that form close contacts in the structure of α-spc SH3. Ten such methyl−methyl pairs, with carbon−carbon distance in the range from 3.6 to 4.2 Å, were selected from the crystallographic structure 1U06. In each case, the simulation included four spins, representing two methyl groups selectively labeled with ^{13}C, ^{1}H. The topology of the spin system was the same as that found in the crystallographic structure.[81] Included in the calculations were dipolar interactions between all spins in the four-spin system, chemical shift evolution, plus the empirical leakage terms modeling the dissipation of the proton magnetization. The chemical shift values were chosen according to the experimental spectra. The magnitude of the generic leakage rate was set to 100 s^{-1}, based on the typical proton line width (ca. 30 Hz).[82] The calculations were carried out assuming the spectrometer frequency of 600 MHz and a MAS frequency of 22 kHz.

The simulated PDSD transfer turned out to be small, in agreement with the experimental findings. For the mixing time of 2.0 s, which corresponds to the longest T_{rel} delay used in our relaxation measurements, the amount of the transferred magnetization was in the range from 0.3 to 7.2%. In reality, the magnitude of the transfer should be even smaller. First, only one of the two methyl groups in the Val and Leu side chains is ^{13}C-labeled. This undercuts the efficiency of the transfer by

(75) Kalk, A.; Berendsen, H. J. C. *J. Magn. Reson.* **1976**, *24*, 343–366.
(76) Ulmer, T. S.; Campbell, I. D.; Boyd, J. *J. Magn. Reson.* **2002**, *157*, 181–189.
(77) Krushelnitsky, A.; Brauniger, T.; Reichert, D. *J. Magn. Reson.* **2006**, *182*, 339–342.
(78) Giraud, N.; Blackledge, M.; Böckmann, A.; Emsley, L. *J. Magn. Reson.* **2007**, *184*, 51–61.
(79) Szeverenyi, N. M.; Sullivan, M. J.; Maciel, G. E. *J. Magn. Reson.* **1982**, *47*, 462–475.
(80) Reif, B.; van Rossum, B. J.; Castellani, F.; Rehbein, K.; Diehl, A.; Oschkinat, H. *J. Am. Chem. Soc.* **2003**, *125*, 1488–1489.

(81) To account for fast methyl rotation, ^{1}H is placed in the geometric center of the three methyl proton (deuterium) atoms. The resulting geometry is used to define dipolar interactions in the four-spin system with the exception of the ^{13}C−^{1}H dipolar interaction across one bond: the strength of this interaction is calculated assuming the bond length $r_{CH} = 1.117$ Å (Ottiger, M.; Bax, A. *J. Am. Chem. Soc.* **1998**, *120*, 12334) and then rescaled by applying the factor $(3\cos^2\theta_{HCC}-1)/2 = -(1/3)$, as appropriate for the rapidly rotating methyl group.

(82) During the calculations, we employed the (automatically generated) product operator basis composed of spin orders and homonuclear ZQ coherences. The empirical relaxation term was applied using the following set of rules: if the spin mode contains no proton operators, then it does not relax; if it contains a single proton operator, I_z, then it relaxes with the decay rate R_{leak}; if it contains a pair of proton operators, I_zS_z or $I_\pm S_\mp$, then it relaxes with the decay rate $2R_{leak}$.

roughly a factor of 2. Second, many of the close contacts found in the structure are formed by the mobile side chains such as Val23. The dipolar interactions in such systems are partially averaged due to the local dynamics, leading to further decline in the transfer efficiency. Finally, the leakage term used in the simulations is likely to be overestimated. Indeed, much of the proton line width comes from the imperfect shimming, sample inhomogeneity, etc. Furthermore, the longitudinal proton magnetization is likely to be dissipated at a slower rate than the transverse one. The decrease in the leakage rate leads to a steep reduction in the PDSD transfer, as discussed below.

To further explore the potential scope of the PDSD effect, the simulations were repeated while varying different variables of interest. The resulting observations can be summarized as follows:

(*i*) In the context of our experiment, the PDSD transfer can be safely neglected if ^{13}C chemical shift difference between the proximal methyls is at least 1 ppm (150 Hz) or higher. Otherwise, if ^{13}C chemical shifts happen to be degenerate, the PDSD transfer is highly efficient and has profound consequences for the outcome of the relaxation experiment.

(*ii*) The high degree of deuteration of the α-ketoisovalerate-derived sample and the resulting modest ^{1}H leakage rate, 100 s^{-1}, are important for keeping the PDSD level low. Otherwise, for fully protonated samples (^{1}H leakage rate 5000 s^{-1}),[68,83] the efficiency of the PDSD transfer increases by approximately 2-fold. Even more significant increases are predicted for the samples with an intermediate protonation level (^{1}H leakage rate 1000 s^{-1}).

(*iii*) The high MAS frequency, 22 kHz, is important for keeping the PDSD level low. Otherwise, for moderately fast MAS (10 kHz), the efficiency of the PDSD transfer increases by approximately 3-fold.

(*iv*) ^{13}C Relaxation in methyls is sufficiently fast so that the relaxation measurements can be conducted using relatively short T_{rel} delays (on the order of 1 s). There is not enough time for the PDSD effect to develop. In contrast, backbone relaxation measurements that use much longer T_{rel} delays are vulnerable to the spin-diffusion effects.[78,84]

(*v*) The efficiency of the PDSD transfer is affected by the topology of the spin system. For example, the linear arrangement, ^{13}C−^{1}H···^{1}H−^{13}C, which is often encountered in the proteins hydrophobic core, shows no appreciable PDSD transfer.

It is worth noting that our specific experiment, which targets methyl ^{13}C relaxation, employs the sparse methyl labeling scheme, and takes advantage of the fast MAS rate, is uniquely suited to meet the conditions (*i*)−(*iv*). While our particular scheme seems to be largely immune to the PDSD effects, generally the proton-driven spin diffusion should be regarded as an issue of major concern for solid-state relaxation measurements.

Potential Complications: Multiexponential Relaxation in Solids. Torchia and Szabo showed that, generally speaking, spin−lattice relaxation in a spinning polycrystalline sample produces multiexponential decay profiles.[69] The fundamental reason for this can be described as follows. Consider an individual crystallite within the solid sample which contains a pair of spins, such as ^{1}H−^{13}C. The projection of ^{1}H−^{13}C dipolar interaction onto the quantization axis z (static magnetic field B_0) is a function of the crystallite orientation. In the context of spin relaxation, only a portion of dipolar interaction that is modulated by internal motion needs to be considered (e.g. in the case of methyl it is the component of ^{1}H–^{13}C interaction that is orthogonal to the rotation axis). The projection of this time-modulated component of the dipolar interaction on z is also a function of crystallite orientation. Depending on the magnitude of this projection, the dipolar interaction can be more efficient or less efficient in causing relaxation transitions between the Zeeman energy levels, $m_z = -1/2$ and $m_z = 1/2$. As a result, each crystallite is characterized by a distinct (orientation-dependent) dipolar relaxation rate. Under these circumstances, the experimentally observed relaxation profile represents a sum of multiple exponential curves, with each curve corresponding to the individual crystallite.

The inspection of Figure 3 (upper row) fails to show any obvious signs of multiexponential behavior, despite the fact that the curves have been recorded well outside the initial slope region. Nevertheless, this problem needs to be fully investigated before any kind of quantitative data analysis is attempted. In their seminal work, Torchia and Szabo[69] presented a complete formalism suited for analysis of methyl relaxation in spinning solids. In the Appendix (Supporting Information), we apply their method to simulate methyl ^{13}C spin−lattice relaxation. The parameters of the simulation were chosen such as to approximate the conditions of our experimental study. As it turns out, (*i*) the relaxation is, in excellent approximation, monoexponential, and (*ii*) the relaxation rates are very well reproduced by the so-called initial slope approximation[38,69] which, in turn, can be reduced to a model-free-type expression.[85,86] We leave it to the interested reader to consult the details of the calculations (see Appendix, Supporting Information). The obtained results are viewed as a justification for the model-free approach to methyl relaxation in solids, which is adopted in the remainder of this paper.

Model-Free Analysis of the Relaxation Data. In the context of solution studies, the model-free expressions for methyl relaxation have been formulated on the basis of the Woessner's results for the three-site jump model.[74,85,87] A similar approach can be worked out for solids (see Appendix, Supporting Information). The resulting spectral densities for the proton−carbon dipolar interaction in the methyl group are:

$$J_{solution}(\omega) = \frac{1}{5}\left\{(1-\alpha S_f^2)\frac{\tau}{1+(\omega\tau)^2} + \alpha S_f^2 \frac{\tau_R}{1+(\omega\tau_R)^2}\right\} \quad (1.1)$$

$$J_{solid}(\omega) = \frac{1}{5}\left\{(1-\alpha S_f^2)\frac{\tau_f}{1+(\omega\tau_f)^2}\right\} \quad (1.2)$$

$$\alpha = \left(\frac{3\cos^2\theta_{HCC} - 1}{2}\right)^2$$

$$1/\tau = (1/\tau_f) + (1/\tau_R)$$

where αS_f^2 is the fast motion order parameter comprising two factors: α that arises from methyl rotation ($\alpha = 1/9$ for canonical tetrahedral geometry, $\theta_{HCC} = 109.47°$) and S_f^2 that reflects other forms of fast dynamics, such as torsional angle fluctuations in the side chain. The expressions in eq 1 suggest that there are two sources of spin relaxation: (*i*) fast local motion with the correlation time τ_f, which is present both in solution and in solid,

(83) van Rossum, B. J.; Boender, G. J.; de Groot, H. J. M. *J. Magn. Reson. Ser. A* **1996**, *120*, 274–277.
(84) Chevelkov, V.; Diehl, A.; Reif, B. *J. Chem. Phys.* **2008**, *128*, 052316.
(85) Lipari, G.; Szabo, A. *J. Am. Chem. Soc.* **1982**, *104*, 4546–4559.
(86) Kay, L. E.; Torchia, D. A. *J. Magn. Reson.* **1991**, *95*, 536–547.
(87) Woessner, D. E. *J. Chem. Phys.* **1962**, *37*, 647–654.

and (*ii*) overall tumbling with the correlation time τ_R, which only occurs in solution. Importantly, the above results are formulated in such a fashion as to incorporate the similarity hypothesis. Indeed, eq 1 suggests that the fast methyl dynamics in solid and in solution are described by the same order parameters, αS_f^2, and the same correlation times, τ_f.

To complete the theoretical framework, the expressions for spectral densities should be complemented with the standard formulas for ^{13}C dipolar relaxation:[73]

$$R_1^{CH} = \frac{1}{12} c_{CH}^2 \{J(\omega_H - \omega_C) + 3J(\omega_C) + 6J(\omega_H + \omega_C)\} \quad (2.1)$$

$$R_1^{CD} = \frac{2}{9} c_{CD}^2 \{J(\omega_D - \omega_C) + 3J(\omega_C) + 6J(\omega_D + \omega_C)\} \quad (2.2)$$

$$R_2^{CH} = \frac{1}{24} c_{CH}^2 \{4J(0) + J(\omega_H - \omega_C) + 3J(\omega_C) + 6J(\omega_H) + 6J(\omega_H + \omega_C)\} \quad (2.3)$$

$$R_2^{CD} = \frac{2}{18} c_{CD}^2 \{4J(0) + J(\omega_D - \omega_C) + 3J(\omega_C) + 6J(\omega_D) + 6J(\omega_D + \omega_C)\} \quad (2.4)$$

where $c_{IS} = -\sqrt{6}(\mu_0/4\pi)\gamma_I\gamma_S\hbar/r_{IS}^3$. These results can be used with either solid- or solution-state spectral densities, as listed in eq 1. The structural parameters needed for evaluating the relaxation rate constants are $\theta_{HCC} = \theta_{DCC} = 109.47°$, $r_{CH} = 1.115$ Å, and $r_{CD} = 1.110$ Å.[73,88] The contributions of eqs 2.2 and 2.4 should be doubled to account for the presence of two deuterons in the $^{13}CHD_2$ methyl group.

Finally, the ^{13}C CSA contribution needs to be included. The issues surrounding this term have been discussed at length by Ishima, Torchia, and co-workers.[73] Their result can be extrapolated to solids in the same fashion as it was previously done for the dipolar terms:

$$R_1^C = \frac{1}{2} c_C^2 \{3J^*(\omega_C)\} \quad (3.1)$$

$$R_2^C = \frac{1}{4} c_C^2 \{4J^*(0) + 3J^*(\omega_C)\} \quad (3.2)$$

Here the interaction constant is $c_C = (2/3)\omega_C\Delta\sigma_C$, with the recommended value $\Delta\sigma_C = 25$ ppm,[73,89] and the spectral density $J^*(\omega)$ is defined by eqs 1.1 and and 1.2 with the parameter α set to $\alpha = 1$. Ishima et al. estimated the errors associated with the assumption of axially symmetric CSA tensor and with the use of the same τ_f value as in eq 2 and found them to be less than several percent of the net relaxation rates. In the context of the present analysis, the effect of these errors is further reduced by an order of magnitude (see below) and, therefore, can be safely ignored.

The similarity hypothesis, as expressed by eq 1, suggests that solution- and solid-state rates differ in only one respect—the former contain a contribution from the overall molecular tumbling, while the latter are free from it. The significance of this contribution, second term in eq 1.1, can be easily estimated. Assuming $S_f^2 = 0.6$, $\tau_f = 50$ ps (typical for Val and Leu side chains at room temperature[73,90]), $\omega_H/2\pi = 600$ MHz, and $\tau_R = 5$ ns, we calculate that the contribution from the overall molecular tumbling into the solution ^{13}C $R_{1,solution}$ rate amounts to a modest 13%. This estimate suggests that the solid- and solution-state rates can indeed be compared in a meaningful fashion (cf. Figure 4a). In the next section, we seek to carefully evaluate and isolate the tumbling contribution. The ultimate goal of this exercise is to produce a cleaner comparison between the two data sets, focusing on the local dynamics.

Subtracting Overall Tumbling. Comparison of eqs 1.1 and 1.2 indicates a straightforward path to subtraction of the overall tumbling. Since τ_f is 2 orders of magnitude shorter than τ_R, we can safely assume that $\tau \approx \tau_f$, and the two terms in eq 1.1 are thus disentangled (the accrued error is on the order of 1%). What remains is to evaluate the second term in eq 1.1 and subtract the corresponding contributions from the experimental $R_{1,solution}$ rates. Evaluating the tumbling term presents no difficulty—the correlation time τ_R can be obtained in a standard fashion from the backbone ^{15}N data, and the order parameter S_f^2 can be extracted with a good accuracy from the methyl ^{13}C $R_{1,solution}$, $R_{2,solution}$ rates (or, in principle, from a set of ^2H relaxation rates).

It should be stressed that the subtraction is a "benign" procedure which is tolerant to errors. Since the entire tumbling term is on the order of 10% of the $R_{1,solution}$ (see the estimate in the previous section), even a substantial error in determination of this term has only a slight impact on the corrected value $R_{1,solution}^{cor}$. Nevertheless, we carefully constructed the subtraction procedure to minimize possible sources of uncertainty. The details of the algorithm are briefly summarized below.

(*i*) The (assumed axially symmetric) rotational diffusion tensor has been determined by means of the standard analysis using ^{15}N data.[91,92] For our particular sample at 20 °C, it turned out that $\tau_R = 5.59$ ns, with the diffusion tensor anisotropy $\eta = D_\parallel/D_\perp = 1.20$.

(*ii*) The effort has been made to include the (moderate) tumbling anisotropy in the subsequent treatment.[92] For this purpose, we defined τ_R^{eff} for each individual methyl group:

$$\tau_R^{eff} = \tau_R\lambda_{aniso} = \tau_R\left(1 - \frac{\eta - 1}{\eta + 2} \cdot \frac{3\cos^2\vartheta - 1}{2}\right)^{-1} \quad (4)$$

where ϑ is the angle between the three-fold methyl symmetry axis (carbon−carbon bond) and the long axis of the diffusion tensor determined in the previous step. The calculations were carried out using the crystallographic coordinates 1U06; for those side chains that are represented by two alternate conformations, the anisotropy factors λ_{aniso} have been averaged accordingly. Generally, it appears that significant conformational disorder appears in less than a half of the side chains[93,94] and, therefore, the use of τ_R^{eff} instead of a generic τ_R should provide a measure of improvement. The effects are, in any event, modest, with the values of λ_{aniso} ranging from 0.97 to 1.07.

(*iii*) The solution-state methyl ^{13}C $R_{1,solution}$ and $R_{2,solution}$ rates were used to fit the model-free parameters S_f^2 and τ_f according to eqs 1.1, 2, and 3. In doing so, τ_R was replaced with the site-specific τ_R^{eff}, as obtained in the previous step.

(*iv*) Finally, the contributions from the overall tumbling into the ^{13}C $R_{1,solution}$ rates were evaluated using the fitted S_f^2 and τ_R^{eff} values. The tumbling contributions were then subtracted from the original solution rates to obtain the set of the corrected rates,

(88) Raynes, W. T.; Fowler, P. W.; Lazzeretti, P.; Zanasi, R.; Grayson, M. *Mol. Phys.* **1988**, *64*, 143–162.
(89) Wylie, B. J.; Franks, T.; Graesser, D. T.; Rienstra, C. M. *J. Am. Chem. Soc.* **2005**, *127*, 11946–11947.
(90) Skrynnikov, N. R.; Millet, O.; Kay, L. E. *J. Am. Chem. Soc.* **2002**, *124*, 6449–6460.
(91) Tjandra, N.; Feller, S. E.; Pastor, R. W.; Bax, A. *J. Am. Chem. Soc.* **1995**, *117*, 12562–12566.
(92) Lee, L. K.; Rance, M.; Chazin, W. J.; Palmer, A. G. *J. Biomol. NMR* **1997**, *9*, 287–298.
(93) Mittermaier, A.; Kay, L. E. *J. Am. Chem. Soc.* **2001**, *123*, 6892–6903.
(94) Chou, J. J.; Case, D. A.; Bax, A. *J. Am. Chem. Soc.* **2003**, *125*, 8959–8966.

$R^{cor}_{1,solution}$. The average magnitude of the correction was 17% (cf. the estimate made in the previous section).

Figure 4b illustrates the correlation between $R^{cor}_{1,solution}$ obtained as a result of the subtraction procedure $(i)-(iv)$ and $R_{1,solid}$. As expected, the bias associated with the overall tumbling is eliminated and the points are aligned essentially along the diagonal. The correlation coefficient improves somewhat from 0.94 in Figure 4a to 0.95 in Figure 4b. In this study, we favor the subtraction scheme because it retains, to the maximum possible degree, the dynamic information encoded in the original $R_{1,solution}$ rates. It is also worth noting that the $R^{cor}_{1,solution}$ values are derived on the basis of *solution data alone*, so that the principle of comparing solid data with the solution data is not compromised.

Role of Side-Chain Rotameric Jumps. The Lipari−Szabo model eq 1 takes into consideration fast local dynamics (most prominently, methyl rotation), but makes no provision for slower motions. In this section, we consider the scenario involving multiple time scales and, specifically, discuss the effect of rotameric jumps involving torsional angles χ_1 and χ_2. Note that these jumps are only relevant for spin relaxation if they connect substantially populated rotameric states.[95]

If the rotameric jumps are fast (comparable to methyl spinning), then they are subsumed into the fast component of the Lipari−Szabo spectral density (eq 1.1). This is often the case for Leu side chains, as manifested by the low order parameters S^2_f.[96] If the jumps are slow (much slower than the protein overall tumbling), then they do not contribute appreciably to $R_{1,solution}$ or $R_{2,solution}$ and, therefore, eq 1.1 remains applicable. Note, however, that S^2_f and τ_f for such side chains represent effective averages over multiple side-chain conformations. In both cases, the procedures $(i)-(iv)$ allow for accurate evaluation and removal of the tumbling term.

The complications arise when the rotameric jumps occur on the time scale comparable with the overall tumbling, τ_R. Fortunately, this does not happen often—only about 10% of methyl-bearing side chains demonstrate this behavior.[90,97] In the case of α-spc SH3, our previous ^{2}H relaxation study showed that all residues are in perfect compliance with the simple two-parameter Lipari−Szabo model (LS-2), with the single exception of Val23.[17] As already mentioned, the presence of conformational disorder in Val23 is confirmed by the X-ray crystallographic structure,[23] as well as ^{2}H MAS line shape analysis.[98]

Cases such as Val23 are interpretable using three-parameter (LS-3) or four-parameter (LS-4) model[90,97,99] in the spirit of the Clore−Lipari−Szabo approach.[100,101] In principle, the procedures $(i)-(iv)$ are no longer valid under these circumstances. In practice, however, it provides a workable approximation. To obtain insight into this problem, we chose the specific example of Val23, for which the LS-4 parametrization is available.[17] The simulation shows that the procedures $(i)-(iv)$ in this case remove the tumbling contribution quite accurately, introducing less than 1.5% error in the resulting $R^{cor}_{1,solution}$ value.

In summary, relatively few of the methyl-bearing side chains fall outside the scope of the LS-2 model in solution. To deal with these special situations, the LS-4 interpretation can be attempted (note that a large amount of data is needed to support such analysis). The effect of the tumbling can be then eliminated by re-defining the expressions for the spectral densities (cf. Chevelkov et al.[18]). Alternatively, the simple approach $(i)-(iv)$ can still be employed to approximately remove the tumbling contribution.

Discussion

The question arises as to how to interpret the result in Figure 4b. One possible point of view is that this result simply reaffirms the similarity between the solution structure and the crystalline structure. In principle, this is a valid point—two identical structures are likely to display very similar dynamics, minor differences in the environment notwithstanding. In reality, however, the relationship between the protein structure and the dynamics of the hydrophobic core is so intricate and subtle that one cannot be viewed as a simple extension of the other.

Mittermaier et al. recognized that there are no simple structural determinants of methyl dynamics in proteins.[102] Such intuitive measures as local packing density or solvent accessibility correlate only weakly with the experimentally measured methyl order parameters. Ming and Brüschweiler constructed a (tunable) model for prediction of order parameters based on structural variables.[103] As it turned out, the model has only modest predictive power, $r \sim 0.55$, and mainly reflects the dependence of the order parameters on the length of the side chain.[96] Mittermaier and co-workers noticed that conserved residues tend to have higher order parameters, $r \sim 0.50$.[104] At the same time, it has been pointed out that one and the same structural fold can accommodate a highly mobile core as well as a relatively rigid one.[105,106]

MD simulations had limited success in reproducing methyl order parameters, with correlation coefficients typically in the range of $r \sim 0.50-0.60$,[96,107,108] although significant improvements were recently reported, $r \sim 0.75-0.85$.[109−111] Best et al. used MD modeling to explore the effect of simple structural perturbations on side-chain dynamics.[96] For this purpose, the authors generated a series of constructs where certain side chains were "frozen" or replaced with more compact analogues. The response of the system proved to be complex, with some residues showing increases in the order parameters and others showing decreases. Similar trends have been observed experimentally. For example, point mutations introduced at different

(95) Wittebort, R. J.; Szabo, A. *J. Chem. Phys.* **1978**, *69*, 1722–1736.
(96) Best, R. B.; Clarke, J.; Karplus, M. *J. Mol. Biol.* **2005**, *349*, 185–203.
(97) Millet, O.; Mittermaier, A.; Baker, D.; Kay, L. E. *J. Mol. Biol.* **2003**, *329*, 551–563.
(98) Hologne, M.; Faelber, K.; Diehl, A.; Reif, B. *J. Am. Chem. Soc.* **2005**, *127*, 11208–11209.
(99) Johnson, E.; Chazin, W. J.; Rance, M. *J. Mol. Biol.* **2006**, *357*, 1237–1252.
(100) Clore, G. M.; Szabo, A.; Bax, A.; Kay, L. E.; Driscoll, P. C.; Gronenborn, A. M. *J. Am. Chem. Soc.* **1990**, *112*, 4989–4991.
(101) Nicholson, L. K.; Kay, L. E.; Baldisseri, D. M.; Arango, J.; Young, P. E.; Bax, A.; Torchia, D. A. *Biochemistry* **1992**, *31*, 5253–5263.
(102) Mittermaier, A.; Kay, L. E.; Forman-Kay, J. D. *J. Biomol. NMR* **1999**, *13*, 181–185.
(103) Ming, D. M.; Brüschweiler, R. *J. Biomol. NMR* **2004**, *29*, 363–368.
(104) Mittermaier, A.; Davidson, A. R.; Kay, L. E. *J. Am. Chem. Soc.* **2003**, *125*, 9004–9005.
(105) Best, R. B.; Rutherford, T. J.; Freund, S. M. V.; Clarke, J. *Biochemistry* **2004**, *43*, 1145–1155.
(106) Barnwal, R. P.; Chaudhuri, T. R.; Nanduri, S.; Qin, J.; Chary, K. V. R. *Proteins: Struct., Funct., Bioinf.* **2006**, *62*, 501–508.
(107) Chatfield, D. C.; Szabo, A.; Brooks, B. R. *J. Am. Chem. Soc.* **1998**, *120*, 5301–5311.
(108) Best, R. B.; Clarke, J.; Karplus, M. *J. Am. Chem. Soc.* **2004**, *126*, 7734–7735.
(109) Hu, H.; Hermans, J.; Lee, A. L. *J. Biomol. NMR* **2005**, *32*, 151–162.
(110) Showalter, S. A.; Brüschweiler, R. *J. Chem. Theory Comput.* **2007**, *3*, 961–975.
(111) Showalter, S. A.; Johnson, E.; Rance, M.; Brüschweiler, R. *J. Am. Chem. Soc.* **2007**, *129*, 14146–14147.

sites in the protein caused virtually no structural change, but nevertheless produced significant changes in side-chain dynamics.[97,112−114] Altering the pH has had the same effect.[115] Not surprisingly, even bigger variations have been observed upon (functionally relevant) ligand binding.[99,116−118]

The relationship between the methyl correlation times τ_f and the structural variables appears to be even more obscure. As pointed out by Chatfield et al.[39,119] and further discussed by Xue et al.,[40] the values of τ_f critically depend on the protein "breathing". An attempt to predict τ_f on a basis of a single coordinate set, even when using ultrahigh resolution crystallographic structures, leads to systematic overestimation of the energy barriers by 1−1.5 kcal/mol, which translates into an order-of-magnitude error in τ_f. Molecular dynamics simulations have done poorly in predicting the values of τ_f, with $r \sim 0-0.4$ for the same-type residues and $r = 0.64$ for all methyl-bearing residues.[39,40,107]

The lack of predictive power with regard to τ_f is especially significant in the context of this study. From eq 1.2, it can be readily appreciated that ^{13}C R_1 rates are only mildly sensitive to variations in S_f^2 but strongly depend on τ_f. The inability to predict τ_f underscores the importance of the experimental approach. The information obtained from the methyl ^{13}C relaxation measurements is nontrivial and cannot be deduced on the basis of the protein structure.

How to judge the correlation coefficient 0.95 obtained in our comparative study (Figure 4b)? As a point of reference, consider typical variations encountered in the *solution* relaxation measurements. A large amount of data is available on methyl ^2H R_1 relaxation, which is controlled by the same variable, τ_f, as ^{13}C relaxation.[73] Kay and co-workers investigated the impact of (structure-conserving) point mutations in protein L and in Fyn SH3 domain.[97,112] The resulting changes in the ^2H R_1 rates typically correspond to $r \sim 0.90$. In certain cases, however, the correlation coefficients can be as low as 0.78 (0.64 when the comparison is limited to Val and Leu side chains). Hu et al. compared the internal dynamics of elgin at pH 3 and 7.[115] The variations between the two sets of ^2H R_1 rates were at the level of $r = 0.90$ for all side chains and 0.93 for Val and Leu only.

We conclude, therefore, that the level of agreement obtained in our comparative study, $r = 0.95$, is on par with what is obtained in the solution experiments involving "minor" structural perturbations. This is indeed highly satisfying, considering that the sample conditions in our solid- and solution-state measurements are different in more ways than one. First, our solution data have been collected on a sample with pH 3.5, whereas the solid-state sample was crystallized from the mother liquor at pH 7.5. Second, the solution sample was prepared using 90% H_2O solvent, while the solid sample was crystallized from 90% D_2O solvent. Of note, substitution of D_2O for H_2O has a stabilizing effect on proteins and is also likely to influence internal dynamics.[120,121] Third, and most important, crystal contacts may contribute to differences in internal dynamics, as discussed above. Indeed, the methyl group Leu8 $\delta 2$, which appears farthest from the diagonal in Figure 4b, is involved in a close crystal contact. Although other methyls are not directly implicated in crystal contacts, they may also be affected given the collective character of the internal dynamics.

Considering all these potential sources of discrepancy, plus the limited precision of the solid-state measurements, the correlation observed in Figure 4b is indeed remarkable. This level of agreement provides an important validation for the new solid-state methodology. It further raises a possibility that solid- and solution-state data can be analyzed in a joint fashion.

Conclusion

Consider for a moment a methyl-bearing side chain that samples multiple conformational states, with rotameric jumps on the nanosecond time scale. In solids, one can distinguish two contributions into the methyl R_1 rates—the one associated with fast methyl rotation and the other that stems from the slow rotameric jumps. Disregarding details, these contributions can be represented as $(8/9)\tau_f$ and $(1/9)(1 - S_s^2)\tau_s/(1 + \omega_C^2\tau_s^2)$, where S_s^2 and τ_s parametrize the slow (nanosecond) motions. Due to the advantage in the motional amplitude, (8/9) versus (1/9), the first contribution is usually dominant. This property makes the methyl ^{13}C R_1 rates particularly well suited for drawing a comparison between the solid- and solution-state data, as demonstrated in this work. A high degree of similarity observed in our study is an interesting result *per se*, but its true significance can be appreciated in the context of other applications.

As an example of such future application, let us consider the methyl ^{13}C R_2 rates. The technical possibility to measure true Redfield R_2 rates in the solid-state MAS experiments has been demonstrated by Akasaka and co-workers.[71,122] In the case of the flexible side chain, the contributions from the fast and slow motional modes into the R_2 rate can be expressed as $(8/9)\tau_f$ and $(1/9)(1 - S_s^2)\tau_s$, respectively. Clearly, the second term has a potential to dominate the rate if τ_s is sufficiently long (with increase in τ_s Redfield theory eventually breaks down; at that point, the peaks are severely broadened). The sensitivity of $R_{2,solid}$ to slower forms of motion creates a unique opportunity to detect the side-chain rotameric jumps *and* to quantify the jump rate in a broad range extending to hundreds of nanoseconds. Our preliminary observations concerning the intensity of signals from Leu31 and Val46 (see Materials and Methods) support the possibility of such study.

One significant problem facing this study is the separation of the fast and slow motional processes. With S_s^2 anywhere from 0.0 to 1.0, the two respective contributions into $R_{2,solid}$ will often be of comparable magnitude. The magnetic field dependence offers little help since the rates are dominated by the $J(0)$ terms. This is the situation where we expect the similarity hypothesis to be useful. Assuming that the side-chain motions are quantitatively (or at least semiquantitatively) similar in solids and in solution, one can undertake a combined analysis of the two respective data sets. While solution-state data are insensitive to long τ_s, they allow for reliable determination of τ_f. Having

(112) Mittermaier, A.; Kay, L. E. *Protein Sci.* **2004**, *13*, 1088–1099.
(113) Clarkson, M. W.; Lee, A. L. *Biochemistry* **2004**, *43*, 12448–12458.
(114) Igumenova, T. I.; Lee, A. L.; Wand, A. J. *Biochemistry* **2005**, *44*, 12627–12639.
(115) Hu, H.; Clarkson, M. W.; Hermans, J.; Lee, A. L. *Biochemistry* **2003**, *42*, 13856–13868.
(116) Kay, L. E.; Muhandiram, D. R.; Farrow, N. A.; Aubin, Y.; Forman-Kay, J. D. *Biochemistry* **1996**, *35*, 361–368.
(117) Finerty, P. J.; Muhandiram, R.; Forman-Kay, J. D. *J. Mol. Biol.* **2002**, *322*, 605–620.
(118) Frederick, K. K.; Marlow, M. S.; Valentine, K. G.; Wand, A. J. *Nature* **2007**, *448*, 325–U3.
(119) Chatfield, D. C.; Augsten, A.; D'Cunha, C.; Wong, S. E. *J. Comput. Chem.* **2003**, *24*, 1052–1058.
(120) Sasisanker, P.; Oleinikova, A.; Weingartner, H.; Ravindra, R.; Winter, R. *Phys. Chem. Chem. Phys.* **2004**, *6*, 1899–1905.
(121) Efimova, Y. M.; Haemers, S.; Wierczinski, B.; Norde, W.; van Well, A. A. *Biopolymers* **2007**, *85*, 264–273.
(122) Krushelnitsky, A.; Kurbanov, R.; Reichert, D.; Hempel, G.; Schneider, H.; Fedotov, V. *Solid State Nucl. Magn. Reson.* **2002**, *22*, 423–438.

evaluated τ_f, one can readily extract τ_s from the solid-state data. Such combined solid/solution study is currently underway in our laboratories.

How general is the similarity hypothesis and to what extent solid-state relaxation data can be combined with solution-state data? We believe that there are certain systems for which the similarity hypothesis is valid and other systems for which it is not. Considering backbone dynamics, the similarity hypothesis may fail in the case of the surface-exposed loops. Indeed, large amplitude motions of the surface loops can be easily arrested by crystal contacts. On the other hand, the similarity hypothesis is expected to hold well for the structured portion of the protein, for example, the extended β-sheet in the case of the α-spc SH3. We have demonstrated that combined analysis of the solid- and solution-state ^{15}N relaxation data leads to new insight into slow (nanosecond) time-scale internal dynamics,[18] consistent with the latest findings from residual dipolar coupling studies.[123,124] Recent observation of transverse cross-correlations by solid-state MAS spectroscopy can potentially enhance this analysis by supplying a reliable R_2-type parameter.[63,125]

Turning to larger systems, we can also envisage different scenarios. For instance, domain−domain motions in a multidomain protein are very likely to be quenched upon crystallization. On the other hand, internal motions in a membrane channel reconstituted in lipids or lipid-like environment are likely to be preserved, irrespective of whether the NMR sample is classified as solid or liquid.[126−129] In a situation like this, combined study of protein dynamics using both solid- and solution-state NMR experiments may prove to be relevant and insightful.

Acknowledgment. This work was supported by the DFG Grant Re1435 to B.R. and the NSF Grant CHE-0723718 to N.R.S.

Supporting Information Available: Appendix describing the analysis of methyl relaxation in spinning polycrystalline samples. Schemes of solution-state pulse sequences for measuring ^{13}C R_1, $R_{1\rho}$ relaxation rates in $^{13}CHD_2$ methyl groups. Assignments of Val and Leu methyl resonances from α-spc SH3 in solid and in solution. Correlation plots for methyl ^{1}H, ^{13}C chemical shifts in solid and in solution. This material is available free of charge via the Internet at http://pubs.acs.org.

JA804275P

(123) Yao, L.; Vögeli, B.; Torchia, D. A.; Bax, A. *J. Phys. Chem. B* **2008**, *112*, 6045–6056.
(124) Lange, O. F.; Lakomek, N. A.; Farès, C.; Schröder, G. F.; Walter, K. F. A.; Becker, S.; Meiler, J.; Grubmüller, H.; Griesinger, C.; de Groot, B. L. *Science* **2008**, *320*, 1471–1475.
(125) Chevelkov, V.; Diehl, A.; Reif, B. *Magn. Reson. Chem.* **2007**, *45*, S156–S160.
(126) Takeuchi, K.; Yokogawa, M.; Matsuda, T.; Sugai, M.; Kawano, S.; Kohno, T.; Nakamura, H.; Takahashi, H.; Shimada, I. *Struct. Fold. Des.* **2003**, *11*, 1381–1392.
(127) Yu, L. P.; Sun, C. H.; Song, D. Y.; Shen, J. W.; Xu, N.; Gunasekera, A.; Hajduk, P. J.; Olejniczak, E. T. *Biochemistry* **2005**, *44*, 15834–15841.
(128) Chill, J. H.; Louis, J. M.; Baber, J. L.; Bax, A. *J. Biomol. NMR* **2006**, *36*, 123–136.
(129) Lange, A.; Giller, K.; Hornig, S.; Martin-Eauclaire, M. F.; Pongs, O.; Becker, S.; Baldus, M. *Nature* **2006**, *440*, 959–962.

Protein side-chain dynamics as observed by solution- and solid-state NMR spectroscopy: a similarity revealed.

Vipin Agarwal,[†] Yi Xue,[‡] Bernd Reif,[†*] Nikolai R. Skrynnikov[‡*]

Supporting Information

† Forschunginstitut für Molekulare Pharmakologie (FMP), Robert-Rössle-Str. 10, 13125 Berlin, Germany

‡ Department of Chemistry, Purdue University, 560 Oval Drive, West Lafayette IN 47907-2084, USA

*Corresponding authors (nikolai@purdue.edu and reif@fmp-berlin.de)

Appendix: methyl relaxation in spinning polycrystalline samples.

Torchia and Szabo presented an elegant formalism for analyzing multiexponential relaxation in spinning solids.[1] They further detailed the initial slope approximation (ISA) where the result is reduced to a single exponential. Remarkably, ISA reproduces the portion of the solution-state relaxation rate which is due to internal molecular dynamics, while omitting the contribution from the overall tumbling. In view of the recent efforts to bridge solid- and solution-state relaxation studies,[2-4] the universal character of the ISA result is especially attractive.

While the ISA approach has been formulated some twenty five years ago, its validity has not been tested until recently.[2] In particular, we addressed this problem in relation to the ^{15}N dipolar-CSA cross-correlated relaxation detected in the solid-state MAS experiments. The calculations establish that the accuracy of the ISA approximation in the situations of practical interest is at the level of several percent.[5, 6] This is far better than the precision of the experimental measurements and, therefore, the ISA analysis is fully applicable to this class of experiments. In the present study we address the same question in relation to the methyl ^{13}C R_1 relaxation.

While a number of sophisticated models are available for dynamics of the methyl-bearing side chains,[7-9] here we restrict ourselves to the simple three-site jump model.[1, 10] Other forms of motion, such as nanosecond time scale rotameric jumps in the side chain, are ignored (see text).

The expressions describing dipolar relaxation in the methyl group which jumps between three symmetric sites can be found in the paper of Torchia and Szabo.[1] Using the same notations as in our recent work,[5] we re-formulate these results as follows:

$$I(t) = \frac{1}{4\pi}\int_0^{2\pi} d\gamma \int_0^{\pi} \sin\beta d\beta \exp\left(-R_1^{cryst}(\beta,\gamma)t\right) \qquad \text{(A1)}$$

$$R_1^{cryst}(\beta,\gamma) = \frac{1}{12} c_{CH}^2 \left\{ J_0(\omega_H - \omega_C) + 3J_1(\omega_C) + 6J_2(\omega_H + \omega_C) \right\} \qquad \text{(A2)}$$

$$J_m(\omega) = v_m(\beta,\gamma)\frac{\tau_\phi}{1+\omega^2\tau_\phi^2} \qquad \text{(A3)}$$

$$v_m(\beta,\gamma) = \sum_{q,q',p=-2}^{2} \left\{ d_{p,m}(\beta_{MAS}) \right\}^2 d_{q,p}(\beta) d_{q',p}(\beta) \cos((q-q')\gamma) \times d_{0,q}(\theta_{HCC}) d_{0,q'}(\theta_{HCC}) \Lambda_{q,q'} \quad \text{(A4)}$$

Here $I(t)$ is the observable relaxation profile, $J_m(\omega)$ is the (orientation-dependent) spectral density, τ_ϕ is the methyl rotation correlation time, $d_{m,m'}(\chi)$ is the reduced second-rank Wigner matrix, and β_{MAS} is the magic angle. The coefficients $\Lambda_{q,q'}$ are equal to one for (q,q') = (-2,-2), (-1,-1), (1,1), (2,2), (-2,1), (-1,2), (1,-2), (2,-1) and otherwise are equal to zero.

When the ISA approximation is applied, these results are rigorously reduced to:

$$I^{ISA}(t) = \exp\left(-R_1^{ISA} t\right) \quad \text{(A5)}$$

$$R_1^{ISA} = \frac{1}{12} c_{CH}^2 \left\{ J(\omega_H - \omega_C) + 3J(\omega_C) + 6J(\omega_H + \omega_C) \right\} \quad \text{(A6)}$$

$$J(\omega) = \overline{v} \frac{\tau_\phi}{1+\omega^2\tau_\phi^2} \quad \text{(A7)}$$

$$\overline{v} = \frac{1}{5}\left\{ 1 - \left(\frac{3\cos^2\theta_{HCC} - 1}{2} \right)^2 \right\} \quad \text{(A8)}$$

If θ_{HCC} is the canonical tetrahedral angle, 109.47º, then $\overline{v}$ evaluates to $8/45$. These results are closely related to the solution-state formula, Eq. (1.1), corresponding to the situation where there is no overall molecular tumbling.

At this point it remains to evaluate the quality of the ISA approximation, Eqs. (A5-A8), in comparison with the rigorous result, Eqs. (A1-A4). For this purpose we simulated a series of relaxation curves $I^{ISA}(t)$ and $I(t)$ based on the mentioned equations. The simulations were conducted for the range of τ_ϕ extending from 10 ps to 150 ps, typical for proteins at around room temperature. The curves were traced to the level of 2% of their initial intensity and sampled on a grid of 10 points uniformly distributed along the t axis. To make the simulations more representative of the experimental study we assumed that the methyls are labeled as $^{13}CHD_2$. Both proton-carbon and deuterium-carbon relaxation terms were included in the calculations.

As it turns out, the agreement between the $I(t)$ and $I^{ISA}(t)$ curves is nearly perfect: the deviation on a point-by-point basis does not exceed 0.00003. When the $I(t)$ profile is fitted with a single exponential, the resulting effective decay rate proves to be within 0.01% of R_1^{ISA}. It is interesting to discuss the reasons for this outstanding level of agreement. Methyl group rotation with $\tau_\phi = 10-150$ ps falls in the extreme narrowing limit, $\omega_H \tau_\phi \ll 1$. Under these circumstances, the expression for R_1^{cryst} becomes proportional to the combination of $v_m(\beta,\gamma)$, $R_1^{cryst} \sim v_0(\beta,\gamma) + 3v_1(\beta,\gamma) + 6v_2(\beta,\gamma)$. Curiously, this combination turns out to be independent of β, γ (although each individual term in it varies strongly as a function of β, γ). Consequently, the integration in Eq. (A1) becomes moot and the results of the rigorous treatment, Eqs. (A1-A4), proves to be exactly equivalent to the ISA results, Eqs. (A5-A8).

It is worthwhile to comment on the quality of the ISA approximation in the situation when methyl spinning is slowed down, $\tau_\phi = 1-100$ ns. The relaxation profile in this case is comprised of many distinct exponentials. Nevertheless, it fits very well with the $\exp(-R_1^{ISA} t)$ curve, such that the error in the effective decay rate does not exceed 0.5%. Note that this result pertains to R_1 relaxation – other relaxation parameters calculated with the same model show more significant deviations. Based on the calculations described above we conclude that the 'solution-style' ISA formulas provide very accurate description for methyl ^{13}C R_1 relaxation in spinning solids. This is a useful finding that facilitates the comparison between the solid- and solution-state methyl ^{13}C R_1 rates.

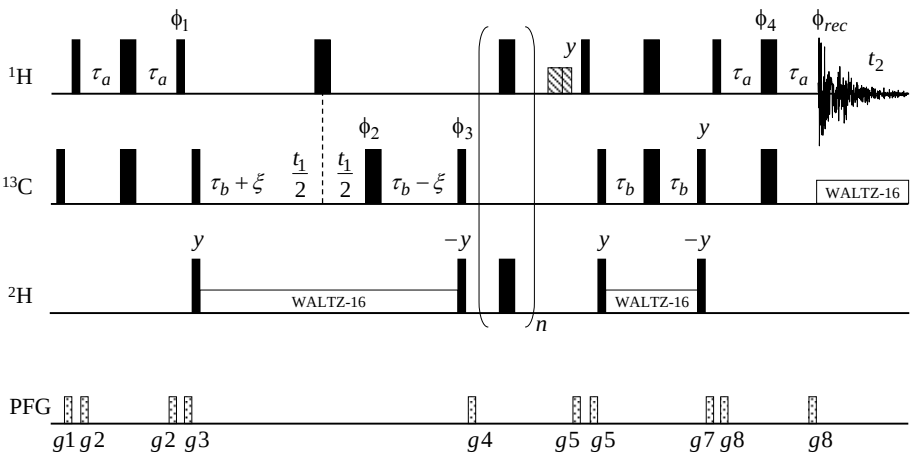

Figure S1a. A solution NMR experiment for measuring carbon R_1 relaxation rates in side-chain methyl $^{13}CHD_2$ groups. The *rf* carriers on the ^{1}H, ^{13}C, and ^{2}H channels were set to 4.8, 24.0, and 0.9 ppm, respectively. Narrow (wide) pulses were applied with a flip angle of 90° (180°) and the field strengths of 45, 16, and 2.5 kHz for the three respective channels. ^{1}H water purge pulses represented by hatched rectangles were applied with the field strength 17 kHz and durations of 6.0 and 3.7 ms.[11] WALTZ-16 decoupling[12] on the ^{13}C and ^{2}H channels was applied with the field strengths of 1.8 and 0.6 kHz, respectively. The cross-correlations were suppressed by application of the ^{1}H and ^{2}H 180º pulses at the rate of one pulse per 250 ms (note that for rapidly relaxing deuterium cross-correlations are expected to be largely self-decoupled).[13, 14] The delays τ_a and τ_b were set to 1.9 ms; the delay ξ was incremented in concert with t_1, changing from 0 to τ_b.[15, 16] The recycling delay between the two consecutive scans was 2 s. The strengths and durations of the gradients were: g1 = (0.5ms, 5G/cm), g2 = (0.3ms, 3G/cm), g3 = (1.5ms, 15G/cm), g4 = (1.0ms, -20G/cm), g5 = (3.0ms, 20G/cm), g6 = (0.5ms, 4G/cm), g7 = (1.0ms, 12G/cm), g8 = (0.125ms, 25G/cm). The spectra were acquired as 576×76 complex matrices with spectral widths of 9000 and 2700 Hz in the ^{1}H and ^{13}C dimensions, respectively. The *rf* pulses have been applied with the phase x, unless indicated otherwise. The phase cycle was ϕ1 = 4(y)4(-y), ϕ2 = (x,y,-x,-y), ϕ3 = y, ϕ4 = 8(x)8(y), ϕ_{rec} =(x,-x,x,-x,-x,x,-x,x,-x,x, -x,x,x,-x,x,-x). Quadrature detection in t_1 was accomplished by States-TPPI[17] of ϕ3. The experimental time per point of the relaxation curve was from 1.5 to 2.5 hrs.

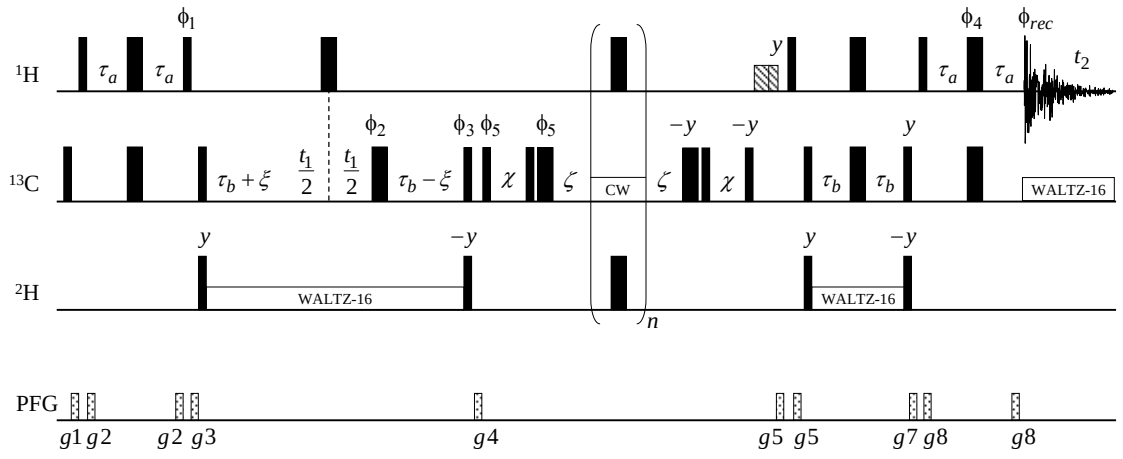

Figure S1b. A solution NMR experiment for measuring carbon $R_{1\rho}$ relaxation rates in side-chain methyl $^{13}CHD_2$ groups. Prior to the *cw* ^{13}C spin-lock period magnetization is aligned with the lock field using the element which compensates for off-resonance effects.[18, 19] The symmetric element is inserted after the spin-lock period. The delays χ and ζ employed in these elements have durations of 61 and 10 μs, respectively. The ^{13}C spin lock with the field strength 2 kHz was applied for the maximum of 160 ms. The recycling delay between the two consecutive scans was 2.8 s. The phase cycle was $\phi1 = 4(y)4(-y)$, $\phi2 = 2(x)2(y)$, $\phi3 = y$, $\phi4 = 8(x)8(y)$, $\phi5 = (y,-y)$, ϕ_{rec} =(x,-x,-x,x,-x,x,x,-x, -x,x,x,-x,x,-x,-x,x). All other experimental settings were the same as described in the caption of Fig. S1a. The experimental time per one point of the relaxation curve was 2 hrs. The measured $R_{1\rho}$ rates were corrected for off-resonance effects in a standard fashion.[20]

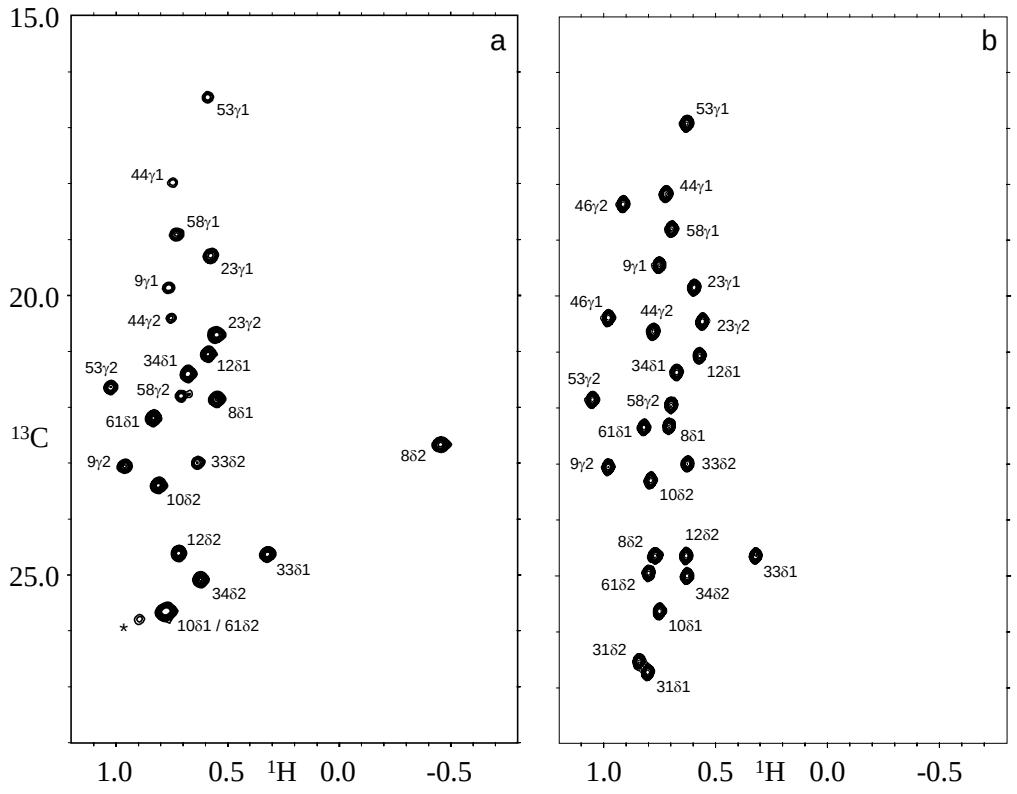

Figure S2. Spectra of α-spc SH3 from methyl ^{13}C R_1 relaxation measurements: (a) pilot solid-state sample and (b) solution-state sample. The previously reported resonance assignments[21-23] have been confirmed using a new TOBSY-based experiment.[24] The tentatively identified resonance from Leu 31 δ2 is marked with an asterisk.

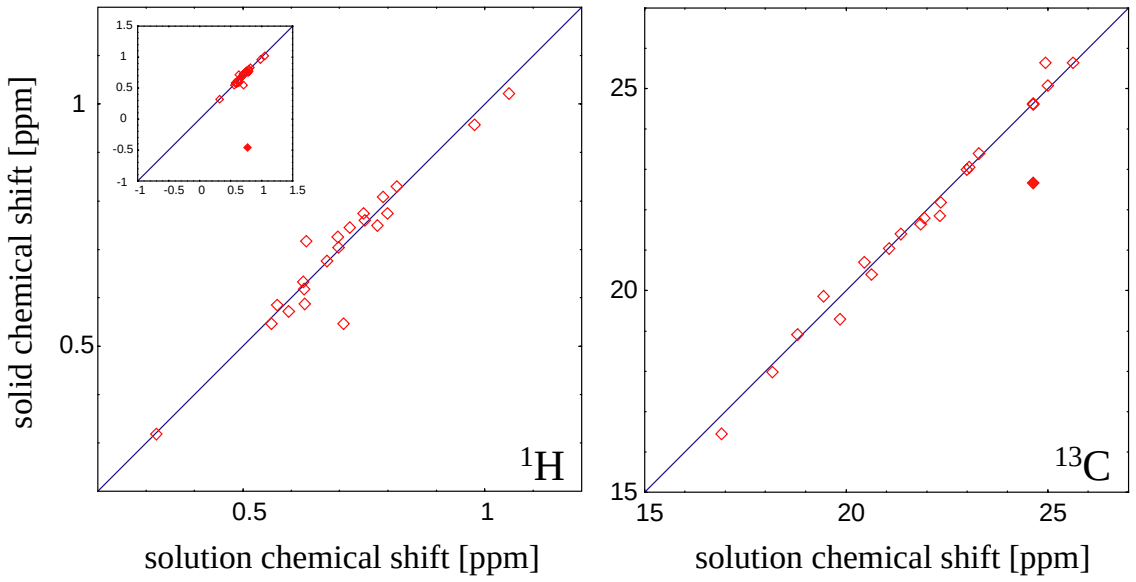

Figure S3. Correlations between methyl chemical shifts in solid- and solution-state spectra of α-spc SH3. The outlier marked by the filled symbol (cf. inset in the left panel) corresponds to the resonance from Leu 8 δ2, which forms a close crystal contact.[22] Included in this graph are the data from the two resonances that are overlapped in the solid-state spectra, Leu 10 δ1 and Leu 61 δ2 (see Fig. S2).

References

(1) Torchia, D. A.; Szabo, A. *J. Magn. Reson.* **1982,** *49*, 107-121.
(2) Giraud, N.; Blackledge, M.; Goldman, M.; Böckmann, A.; Lesage, A.; Penin, F.; Emsley, L. *J. Am. Chem. Soc.* **2005,** *127*, 18190-18210.
(3) Reif, B.; Xue, Y.; Agarwal, V.; Pavlova, M. S.; Hologne, M.; Diehl, A.; Ryabov, Y. E.; Skrynnikov, N. R. *J. Am. Chem. Soc.* **2006,** *128*, 12354-12355.
(4) Chevelkov, V.; Zhuravleva, A. V.; Xue, Y.; Reif, B.; Skrynnikov, N. R. *J. Am. Chem. Soc.* **2007,** *129*, 12594-12595.
(5) Skrynnikov, N. R. *Magn. Reson. Chem.* **2007,** *45*, S161-S173.
(6) Chevelkov, V.; Faelber, K.; Schrey, A.; Rehbein, K.; Diehl, A.; Reif, B. *J. Am. Chem. Soc.* **2007,** *129*, 10195-10200.
(7) Daragan, V. A.; Mayo, K. H. *Prog. NMR Spectrosc.* **1997,** *31*, 63-105.
(8) Choy, W. Y.; Shortle, D.; Kay, L. E. *J. Am. Chem. Soc.* **2003,** *125*, 1748-1758.
(9) Del Rio, A.; Anand, A.; Ghose, R. *J. Magn. Reson.* **2006,** *180*, 1-17.
(10) Woessner, D. E. *J. Chem. Phys.* **1962,** *37*, 647-654.
(11) Messerle, B. A.; Wider, G.; Otting, G.; Weber, C.; Wüthrich, K. *J. Magn. Reson.* **1989,** *85*, 608-613.
(12) Shaka, A. J.; Keeler, J.; Frenkiel, T.; Freeman, R. *J. Magn. Reson.* **1983,** *52*, 335-338.
(13) Palmer, A. G.; Skelton, N. J.; Chazin, W. J.; Wright, P. E.; Rance, M. *Mol. Phys.* **1992,** *75*, 699-711.
(14) Kay, L. E.; Nicholson, L. K.; Delaglio, F.; Bax, A.; Torchia, D. A. *J. Magn. Reson.* **1992,** *97*, 359-375.
(15) Logan, T. M.; Olejniczak, E. T.; Xu, R. X.; Fesik, S. W. *J. Biomol. NMR* **1993,** *3*, 225-231.
(16) Grzesiek, S.; Anglister, J.; Bax, A. *J. Magn. Reson. Ser. B* **1993,** *101*, 114-119.
(17) Marion, D.; Ikura, M.; Tschudin, R.; Bax, A. *J. Magn. Reson.* **1989,** *85*, 393-399.
(18) Yamazaki, T.; Muhandiram, R.; Kay, L. E. *J. Am. Chem. Soc.* **1994,** *116*, 8266-8278.
(19) Hansen, D. F.; Kay, L. E. *J. Biomol. NMR* **2007,** *37*, 245-255.
(20) Davis, D. G.; Perlman, M. E.; London, R. E. *J. Magn. Reson. Ser. B* **1994,** *104*, 266-275.
(21) Pauli, J.; Baldus, M.; van Rossum, B.; de Groot, H.; Oschkinat, H. *ChemBioChem* **2001,** *2*, 272-281.
(22) van Rossum, B. J.; Castellani, F.; Rehbein, K.; Pauli, J.; Oschkinat, H. *ChemBioChem* **2001,** *2*, 906-914.
(23) Agarwal, V.; Diehl, A.; Skrynnikov, N.; Reif, B. *J. Am. Chem. Soc.* **2006,** *128*, 12620-12621.
(24) Agarwal, V.; Reif, B. *J. Magn. Reson.* **2008,** *194*, 16-24.